Article:
Peretti, G., Bouscharain, N. and Dwyer-Joyce, R.S. (2026) In-situ measurement of temperature and pressure in fluid films using ultrasound. Engineering Integrity Journal, 60. pp. 14-20. ISSN: 1365-4101

https://doi.org/10.5281/zenodo.18622414

ENGINEERING INTEGRITY, VOLUME 60, MARCH 2026, pp.14–20. ISSN 1365-4101/2026
DOI: 10.5281/zenodo.18622414

Gladys Peretti was the winner of the 2025 Peter Watson Prize, see page 11.

Technical Paper:

In-Situ Measurement Of Temperature And Pressure In Fluid Films Using Ultrasound

G. Peretti[1], N. Bouscharain[2], R. Dwyer-Joyce[1]
[1]The Leonardo Centre for Tribology, The University of Sheffield, Sheffield, United Kingdom
[2]INSA Lyon, CNRS, LaMCoS, UMR5259, 69621 Villeurbanne, France
Author correspondence: gladys.peretti@sheffield.ac.uk

ABSTRACT

Measuring and controlling temperature and pressure is of paramount importance to ensure safe and thriving conditions for life, and reliable operation for machines and processes. Conventional measurement techniques are seldom suited to confined environments and tribological contacts. This work aims to enable in-situ measurement of temperature and the pressure of any confined liquid layer. To achieve this, an ultrasonic viscosity measurement device equipped with a matching layer was repurposed. Changes in the operating conditions caused the expansion and compression of the matching layer, in turn causing a time shift of the ultrasonic signal. The temperature range spanned from 20 °C to 60 °C, while pressures were measured from ambient pressure up 600 MPa. It is further proposed that tailoring the material of the matching layer to the expected operating conditions can enhance both the sensitivity and accuracy of the measurements.

Nomenclature

Table 1 is a nomenclature of the symbols used in this work.

Symbol	Unit	Parameter
c	m s^{-1}	Shear speed of sound
E	Pa = kg m^{-1} s^{-2}	Young's modulus
f	Hz	Frequency
G	S Pa = kg m^{-1} s^{-2}	Shear modulus
l	m	Layer thickness
n	-	Integer
p	Pa = kg m^{-1} s^{-2}	Pressure (between ambient pressure and 600 MPa in this work)
T	°C	Temperature (between 20 °C and 60 °C in this work)
t	s	Time
z	Rayl = kg s^{-1} m^{-2}	Shear acoustic Impedance
α	-	Thermal expansion coefficient
ν	-	Poisson's ratio
ρ	kg m^{-3}	Density
LDPE	-	Low-density polyethylene

1. Introduction

Measuring temperature and pressure is of prime importance in many fields, from engineering and manufacturing to science and everyday life. These variables impact how materials and living things behave and how systems perform. Controlling both parameters ensures safety, process efficiency and repeatability, as well as economic and environmental gains. This work focuses on confined liquid layers.

Many different methods of **temperature measurements** have been developed and used. The selection of a method is generally driven by the temperature range and precision needed, the state of matter of the medium, physical limitations, such as access to the medium, and finally the cost and ease of use of the method [1]. Some common devices are presented. Liquid-in-glass thermometers rely on the thermal expansion of a liquid in a capillary. They are easy to read and require the capillary to be immersed in the medium. Thermocouples are based on the measurement of a voltage difference between two metal tips [2]. They operate on a wide temperature range, are inexpensive, and can be fitted to small and difficult to access elements. Infrared optical cameras capture the thermal radiations emitted by matter and link it to temperature [3]. They provide a measurement without direct contact to the medium but necessitate direct line of sight. They are used in environments that present a danger (e.g. strong electrical fields), that have moving parts, or in medicine. Additional methods and devices have been developed for specific applications: for example, gases at high temperatures [4]. However, the measurement of temperature in confined environments or tribological contacts, such as in bearings, remains a challenge.

Similar to temperature, **pressure measurements** can be performed using a range of different devices depending on the application. Piezoelectric and capacitive sensors rely on the deformation of a solid, which is then converted to a voltage or capacitance difference [5]. Resonant sensors rely on change of the oscillation frequency as pressure changes. Recent works focused on the miniaturisation of pressure sensors for medical applications, especially to measure blood pressure [6].

A novel approach needs to be developed to measure changes in operating conditions in confined environments and tribological contacts. Ultrasonic waves have been widely used in medicine, as well as in engineering to detect defects in materials or assess coupling between parts [7]. Moreover, ultrasound has been used in the measurement of media properties,

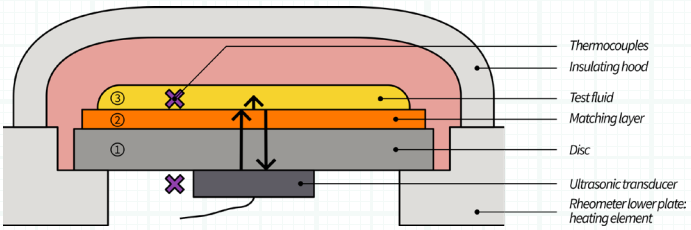

Figure 1: The ultrasonic viscometer in a temperature chamber.

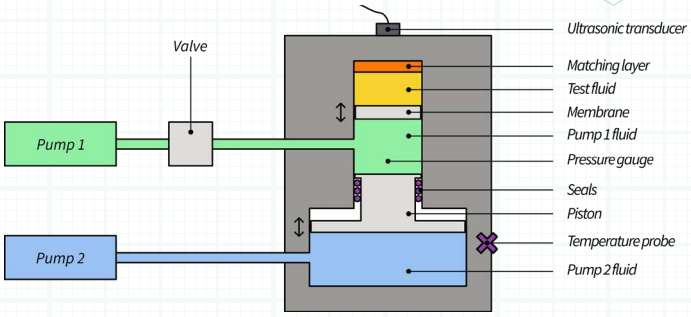

Figure 2: The ultrasonic viscometer in a high-pressure cell.

such as layer thickness [8], sound velocity [9], or attenuation [10]. In particular, shear ultrasonic waves have been used since the mid-20th century to measure fluid viscosity, first with an immersed quartz crystal [11, 12], and then with the ultrasonic transducer separated from the fluid by a test piece [13, 14, 15, 16]. Later on, Schirru [17] introduced a matching layer to acoustically match the solid layer and the fluid and improve the sensitivity.

The aim of this work is to reuse the existing ultrasonic viscometer and assess the possibility of measuring both in-situ temperature and pressure in a tribological contact.

2. Principle And Materials

2.1 Apparatus & Fluids

The pre-test methodology is based on the **ultrasonic viscometer** [18, 19], which comprises four elements:

- The **shear ultrasonic transducer** can be a commercial or a bare piezoelectric element, with the latter preferred here for its small form factor (≈ 5mm width).
- The **test piece** is originally in contact with the fluid and is generally a metal (steel in this work).
- The **matching layer** is a thin layer whose role is to acoustically match the metal and the fluid. To do so, it is chosen so that $z_2 = \sqrt{z_1 z_3}$, with z_1, z_2, z_3 the shear acoustic impedances of the test piece, the matching layer, and the fluid, respectively. In this work, the matching layer was polyimide [20], and its shear acoustic impedance was $z_2 = 1.1$ MRayl. For viscosity measurements, the thickness of the matching layer l_2 dictates the resonance frequency f of the system: $f = \frac{nc_2}{4l_2}$ with n being an integer and c_2 the shear speed of sound in the matching layer. In this work, l_2 is equal to 25 µm or 50 µm.
- The **fluid** to be measured.

This section describes two different setups: one for the evaluation of temperature, the other for pressure measurements.

The first setup was a **temperature-controlled** chamber containing the ultrasonic system (Figure 1). A 6.7mm thick disc of steel was instrumented on one side with a 25 µm thick matching layer made of polyimide, and on the other side with a 10 MHz shear ultrasonic transducer. The temperature control was achieved in a rheometer to obtain a 0.01 °C precision. Two thermocouples were used to control the temperature: one was positioned to measure the fluid temperature on the upper side of the disc, the other measured the temperature of the lower side of the disc.

Viscosity calibration standard lubricants were used for the temperature experiment. These fluids are mineral oils and are considered Newtonian. N10, N14, N26, N35, S6 and S20 are manufactured by Cannon [21], while 85083.260, 85093.260, and 85099.260 are manufactured by VWR [22]. Measurements were performed at 20 °C, 40 °C and 60 °C. Reference measurements were performed at each temperature using air instead of a lubricant.

The second setup was a **high-pressure** cell hosted at AC2T in Austria (Figure 2). It was designed to withstand pressures up to 1.3 GPa. The cell was instrumented with a 50 µm thick polyimide matching layer, and a 8 MHz shear ultrasonic transducer. The temperature regulation was performed by a heating collar. The fluid temperature could not be measured directly because of the tightly closed pressurised environment. A temperature probe on the outside of the cell was thus used, and the cell was allowed several hours to reach temperature equilibrium before capturing any data. The pressure was controlled by two manual pumps and a piston that served as a pressure amplifier. A high-pressure gauge (P3MB BlueLine from HBK) was used to record the pressure data. Viscosity measurements on this rig are described in [19].

Fluids with a well-characterised viscosity behaviour under pressure were used: water, octane, squalane (SQL), 85% squalane + 15% polyisoprene in weight (SQL+PIP), diisodecylphtalate (DidP), and polyalphaolefin 100 (PAO100). The measurements were performed at 40 °C, and from ambient pressure up to 600 MPa. Signals were acquired continuously for ~ 10 minutes for each pressure step. A reference point was captured with air at ambient pressure.

Experiment	Matching layer thickness ($_{\mu}$m)	Frequency (MHz)	Number of cycles	Peak-to-peak amplitude (V)
Temperature	25	7 to 13	10	4
Pressure	50	4.5	5	4

Table 2: Input wave parameters for both apparatus.

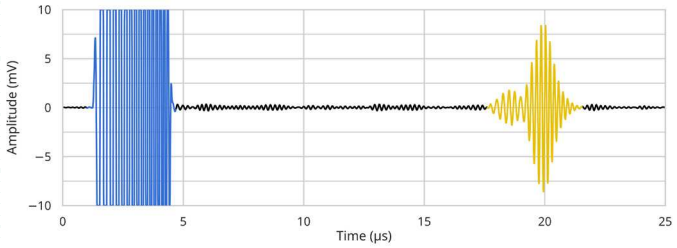

Figure 3: Ultrasonic signal (AScan): input wave in blue, reflected wave in yellow.

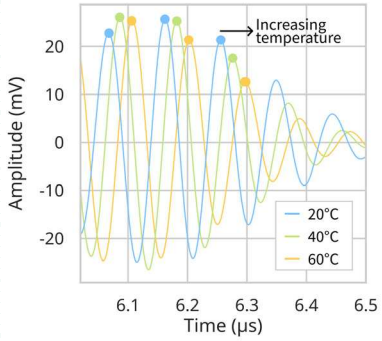

Figure 4: Peak tracking for fluid N10 at 20 °C, 40 °C and 60 °C.

signals to identify the first three peaks. Circle markers are added to the figure to evidence their position.

The time shift is then computed as the position of the peaks for each fluid minus the position of the peaks for air at 20 °C. The three peaks are averaged to give a single value per fluid. The time shift is plotted in nanoseconds as a function of temperature in Figure 5.

The air reference at 20 °C is the baseline; its time shift is equal to 0. As the temperature increases, the time-of-flight of the ultrasonic wave increases, leading to a

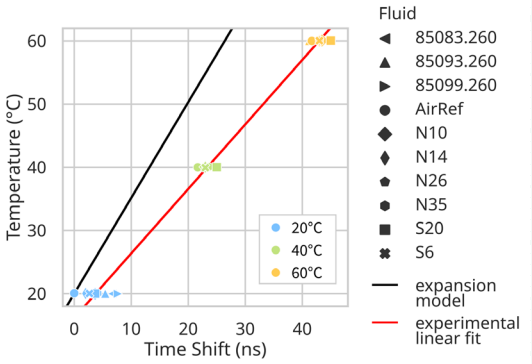

Figure 5: Time shift of the AScans as a function of temperature.

2.2 Acquisition

A waveform generator excited the ultrasonic transducer, thus generating a shear ultrasonic wave. The parameters of the input waves are described in Table 2. The wave travelled through the test piece and the matching layer. At the interface between the matching layer and the fluid, the wave was partly transmitted and partly reflected. The reflected portion was measured by the same ultrasonic transducer (pulse-echo mode). This reflected wave was sensitive to the properties of the fluid; in particular, viscosity can be derived from the signal in the frequency-domain. The aim of this work was to determine if the wave was additionally sensitive to the operating conditions. The ultrasonic signals in the time-domain are called AScan, an example of which is presented in Figure 3.

3. Impact of Temperature on the AScan

In Figure 4, the AScans of fluid N10 at different temperatures are plotted. The three signals appear to exhibit a time shift, with the 20 °C signal to the left, the 40 °C one in the middle, and the 60 °C one to the right. The time shift is due to the matching layer expanding with increasing temperature. A **peak tracking** function (*find_peaks* from Scipy in Python) is applied to the positive time shift. The maximum time shift across the 40 °C temperature range is ≈ 40 ns, which is an order of magnitude greater than the capture resolution of 2 ns, confirming the experimental apparatus is capturing a time shift.

Several challenges in the peak tracking have been encountered; they highlight that the time-shift algorithm should be refined:

- It is difficult to define a single rule to capture the same peaks for all fluids.
- The time between each peak for one fluid is not uniform. It means that the number of selected peaks (three here) affects the value of the computed time shift.
- There is a time shift of up to 8 ns between the air reference and the other fluids at 20 °C. Whether this is due to measurement uncertainty or to the presence of a fluid on the matching layer is unclear.

A **simple expansion model** was built to understand the source of the time shift. To do so, the time-of-flight of the shear ultrasonic wave through the ultrasonic system was computed. The wave was emitted by the ultrasonic transducer, travelled through 6.7 mm of

Property	Original Value	Impact of Temperature
Young's modulus E	known	$E = aT + b$
Poisson's ratio ν	known	–
Thermal expansion coefficient α	known	–
Thickness l	known	$\Delta l = \alpha l_0 \Delta T$
Density ρ	known	$\rho = \frac{\rho_0}{1+\alpha\Delta T}$
Shear modulus G	$G = \frac{E}{2(1+\nu)}$	✓
Shear velocity c	$c = \sqrt{\frac{G}{\rho}}$	✓
Time of flight t	$t = \frac{2l}{c}$	✓

Table 3: Parameters of the time-of-flight model and dependence to temperature.

steel and 25 µm of polyimide matching layer, and returned to the transducer. When submitted to temperature variations, several media properties were temporarily modified: the Young's modulus $E = aT + b$, the thickness $\Delta l = a l_0 \Delta T$ and the density $\rho = \frac{\rho_0}{1+\alpha\Delta T}$ with a, b media-specific constants, and α the thermal expansion coefficient. The shear modulus, the shear velocity, and the time of flight could thus be computed to take into account the impact of temperature. The model parameters are summarised in Table 3. Assuming the media are known, then the original values at 20 °C for the Young's modulus, the Poisson's ratio, the thermal expansion coefficient, the thickness and the density are known.

The expansion model is then compared with the experimental data. In Figure 5, the theoretical time shift is plotted with a solid black line, while the linear fit of the experimental data is plotted with a red line. Both lines follow the same trend, with the time shift increasing linearly with temperature, although the model exhibits lower values. The observed discrepancy can be attributed to peak tracking algorithm limits, and limited time resolution. The systematic error can also be attributed to a gap between the material properties used in the model and those of the actual experimental layers. In the model, both the steel test piece and the matching layer are considered homogeneous. In the experiment, the materials are not perfect, and there is additionally a glue layer, which has been neglected in the model. It should be noted that the linear expansion of the matching layer is only valid on a limited range of temperatures; the model does not yet take this behaviour into account.

The results in this section showed that a change in temperature leads to a time shift. Consequently, the matching layer expansion can be used as an **ultrasonic temperature transducer**.

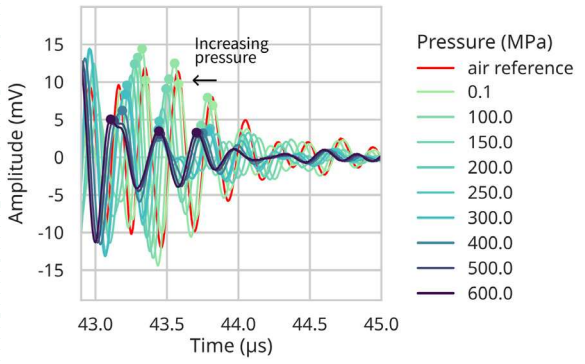

Figure 6: Peak tracking for fluid SQL under pressure.

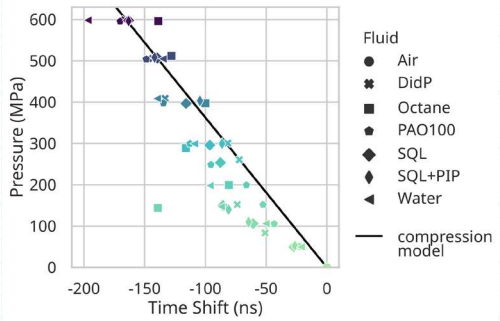

Figure 7: Time shift of the AScans as a function of pressure.

4. Impact of Pressure on the AScan

In Figure 6, the AScans of SQL at different pressures (blue shades) are compared with the air reference (in red). The darker curves, corresponding to the highest pressures, are the furthest to the left, seemingly indicating a time shift as the pressure increases. A **peak-tracking** function (*find_peaks* from Scipy in Python) is applied to the signals to identify the first three peaks. Circle markers are added to the figure to evidence their position.

The **time shift** is then computed as the position of the SQL peaks minus the position of the air reference peaks. Two averages are performed: the first one to average the three time shifts from each signal; the second one to average the time shifts across all the signals from the same pressure step. The averaged time shifts for all fluids are then plotted in nanoseconds as a function of pressure in Figure 7.

The air reference at ambient pressure is the baseline; its time shift is equal to 0. As the pressure increases, the time-of-flight of the ultrasonic wave decreases, leading to a negative time shift. For each pressure step, the time shift variation between all fluids is less than 50 ns. As the pressure increases, the absolute value of the time shift increases. The resolution of the capture is 2 ns; the experimental apparatus is thus accurately capturing a time shift. Some points do not sit on the general trend, for example octane at 150 MPa. This is due to the difficulty of accurately tracking the first three peaks for all lubricants, as can be seen in Figure 6 with a new peak appearing between peaks 2 and 3.

Similarly to the previous expansion model, a **simple compression model** taking into account the impact of pressure on the time-of-flight of the waves was developed. The wave was emitted by the ultrasonic transducer, travelled through 70 mm of steel and 50 µm of polyimide matching layer, and returned to the transducer. The time-of-flight was $t = \frac{2l}{c}$, with l being the media thickness, and c the snear velocity. When submitted to pressure, the thickness of each media was temporarily modified according to $l = l_0 \frac{E-p}{E}$, where l is the thickness under pressure, l_0 the original length, $-p$ the compressing pressure, and E the Young's modulus. The impact of pressure on other parameters (Young's modulus, Poisson's ratio, density, shear modulus and

Property	Original value	Impact of pressure
Young's modulus E	known	–
Poisson's ratio ν	known	–
Thickness l	known	$l = l_0 \frac{E-p}{E}$
Density ρ	known	–
Shear modulus G	$G = \frac{E}{2(1+\nu)}$	–
Shear velocity c	$c = \sqrt{\frac{G}{\rho}}$	–
Time of flight t	$t = \frac{2l}{c}$	✓

Table 4: Parameters of the time-of-flight model and dependence to pressure.

Property	Steel	Polyimide	LDPE
Thickness l (m)	6.7e-3	50e-6	50e-6
Young's modulus E (MPa)	200e3 @20 °C 190e3 @200 °C	2.76e3 @23°C 2e3 @200 °C	200 @20 °C 70 @60 °C
Thermal expansion coefficient α (K^{-1})	1.2e-5	2e-5	2e-4
Poisson's ratio ν	0.3	0.34	0.45
Density p (kg m^{-3})	7800	1420	920
Shear speed of sound c (m s^{-1})*	3132	801	975
Shear acoustic impedance z (Rayl)*	24e6	1.1e6	0.9e6

Table 5: Media properties at 20 °C unless specified. * denotes computed values.

shear velocity) was neglected. The model parameters are summarised in Table 4. Assuming the media are known, then the original values for the Young's modulus, the Poisson's ratio, the thickness, and the density are known. Using these assumptions, the relationship between time-shift and pressure was linear.

The matching layer was made of polyimide, which is a low-stiffness material: its elastic modulus is 80 times lower than that of steel. As a result, it was more impacted by pressure. At 40 °C, if the pressure increased from ambient pressure to 600 MPa, the model predicted a near 25% thickness compression of the matching layer, while the steel part was compressed by less than 0.3%. This meant the matching layer was very sensitive to any pressure changes.

The compression model was then compared with the experimental data. In Figure 7, the theoretical time shift is plotted with a black straight line at 40 °C. The model is in agreement with the experimental data. Neglecting the impact of pressure on most parameters but the thickness yields a first approximation of the time shift. However, the linear compression of the matching layer is only valid on a limited range of pressures; the model does not yet take into account this behaviour.

The results in this section showed that a change in pressure leads to a time shift. Consequently, the matching layer compression can be used as an **ultrasonic pressure transducer**.

5. Optimising the Matching Layer for the Operating Conditions

Polyimide has been used experimentally as a matching layer material because it acoustically matches steel and fluids and because it is commercially available in thin films. To explore the influence of the matching layer material on time shift, a new material with a similar shear acoustic impedance but a different Young's modulus was selected. Low-density polyethylene (LDPE) was chosen, as it is a common plastic, and its material properties can easily be estimated. The values used to define the materials are given in Table 5. It should be noted that the actual values for LDPE will vary depending on the material. Moreover, LDPE has not been used experimentally as a matching layer: the manufacturing of a thin layer and its bonding to the metal surface might be challenging. Finally, the compatibility of LDPE with fluids under high temperatures and pressures has not been assessed. Therefore, the comparison presented below aims to provide qualitative insight into the time-shift behaviour rather than quantitative accuracy.

Using the values provided in Table 5, the expansion and compression models were computed from 20 °C to 60 °C, and ambient pressure up to 600 MPa. The isobars are plotted in Figure 8 for both matching layers. For **polyimide**, the time shift appears to be linear with temperature, whatever the pressure. The time shift increases with temperature and decreases with pressure.

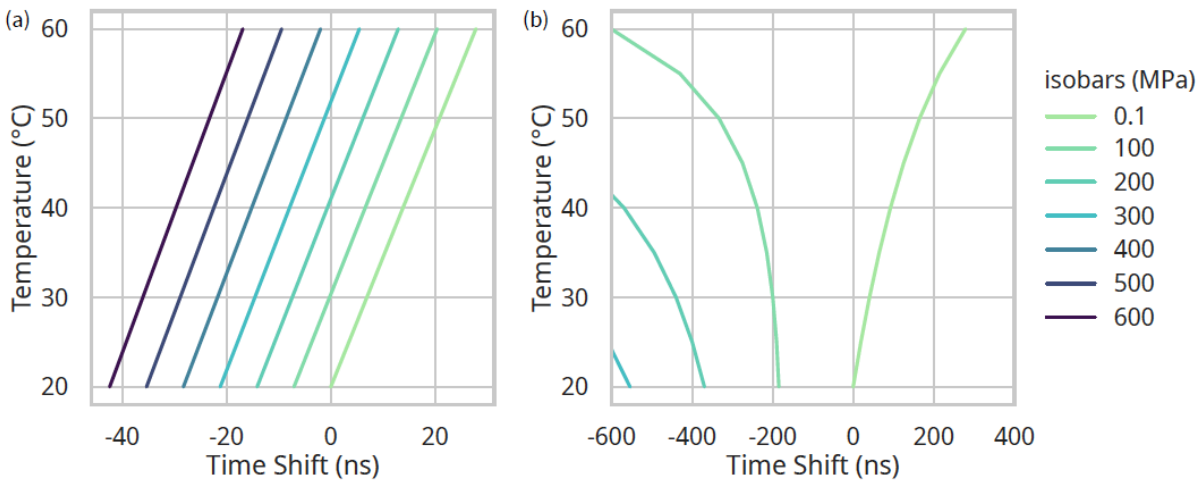

Figure 8: Time shift comparison for two matching layers: (a) polyimide, (b) LDPE.

The total time shift on the whole range of operating conditions is 67 ns.

For **LDPE**, the time shift behaves very differently. First, it is no longer linear with temperature. Second, the isobars are not parallel anymore, with only the ambient temperature curve having a positive slope. Finally, the total time shift on the whole range of operating conditions is 1387 ns, which is considerably larger than for polyimide.

However, the model fails to limit the compression of this matching layer and ends up with negative thicknesses, which is of course impossible. This means that the time shift error increases as the pressure increases. This causes the unexpected shape of the isobars. Looking only at the data at ambient pressure, the time shift is 279 ns, which is still larger than what was obtained with polyimide. LDPE has a lower stiffness than polyimide: it expands and compresses more and is thus more sensitive to the operating conditions. It is therefore confirmed that changing the properties of the matching layer makes it more sensitive to certain temperature and pressure ranges.

The measurements in this work focused on temperatures from 20 °C up to 60 °C, and pressures from ambient pressure up to 600 MPa. In lubricated contacts, temperatures and pressures may extend beyond these ranges. The behaviour of the matching layer is expected to be extrapolated to wider ranges of temperature and pressure, within limits defined by the matching layer material.

The time resolution of the acquisition is a limit to the temperature and pressure resolutions. In this work, the ultrasonic acquisition device was a PicoScope 5444B, which offered a 2 ns time resolution. For the polyimide matching layer, it corresponded in theory to a minimum temperature resolution of 3 °C and 32 MPa. The time resolution could be improved by using a different acquisition device or by changing the matching layer. For the LDPE matching layer, the temperature resolution would be 0.6 °C and that of pressure would be 1.2 MPa. To conclude, the use of a stiffer material is recommended for lower resolution on a wider range of operating conditions. Conversely, a material with a lower stiffness will provide higher resolution on a smaller range of operating conditions.

6. Conclusion

While various devices offer temperature and pressure measurements, few can perform these in confined environments. The aim of this work was to use an ultrasonic device coupled with a matching layer to perform in-situ temperature and pressure measurements. The matching layer is a thin layer of polymer.

• Temperature and pressure increase → expansion and compression of the matching layer (few micrometers → increase and decrease of the time of flight of the ultrasonic wave (few nanoseconds) → time shift correlated with the operating conditions.

• In this work, temperatures from 20 °C to 60 °C, and pressures from ambient up to 600 MPa were measured. The advantage of this method is its use in-situ, opening new perspectives for confined environments such as tribological contacts.

• The material and thickness of the matching layer can be tailored to the ranges of expected temperatures and pressures to provide improved accuracy.

• The in-situ temperature, pressure and viscosity of the fluid can be measured simultaneously to provide detailed information about the system.

ACKNOWLEDGEMENTS

This work was carried out as part of the COMET Centre InTribology project (FFG no. 906860). InTribology is funded within the COMET – Competence Centres for Excellent Technologies Programme by the federal ministries BMIMI and BMWET as well as the federal states of Niederösterreich and Vorarlberg based on financial support from the project partners involved. COMET is managed by FFG.

REFERENCES

[1] P. R. Childs, J. R. Greenwood, and C. A. Long. "Review of temperature measurement". *Review of Scientific Instruments* 71 (8 Aug. 2000), pp. 2959–2978. DOI: 10.1063/1.1305516.

[2] D. D. Pollock. *Thermocouples. Theory and Properties.* 1st ed. Routledge, 1991, p. 336. DOI: 10.1201/9780203735824.

[3] D. P. DeWitt and G. D. Nutter. *Theory and Practice of Radiation Thermometry.* Wiley, 1988. DOI: 10.1002/9780470172575.

[4] A. B. Murphy and A. J. Farmer. "Temperature measurement in thermal plasmas by Rayleigh scattering". *JPhys.D: Applied Physics* 25 (4 Apr. 1992), p. 634. DOI: 10.1088/0022-3727/25/4/009.

[5] J. Fraden. "Handbook of modern sensors: Physics, designs, and applications". *Handbook of Modern Sensors: Physics, Designs, and Applications* (Jan. 2016), pp. 1–758. DOI: 10.1007/978-3-319-19303-8.

[6] P. Song et al. "Recent Progress of Miniature MEMS Pressure Sensors". *Micromachines* 2020, Vol. 11, Page 56 11 (1 Jan. 2020), p. 56. DOI: 10.3390/MI11010056.

[7] J. Krautkrämer and H. Krautkrämer. *Ultrasonic Testing of Materials.* Springer Berlin Heidelberg,1990. DOI: 10.1007/978-3-662-10680-8.

[8] R. Dwyer-Joyce, B. Drinkwater, and C. Donohoe. "The measurement of lubricant film thickness using ultrasound". *The Royal Society* (2002). DOI: 10.1098/rspa.2002.1018.

[9] P. Dou et al. "Simultaneous measurement of thickness and sound velocity of porous coatings based on

the ultrasonic complex reflection coefficient". *NDT & E International* 131 (Oct. 2022), p. 102683. DOI: 10.1016/J.NDTEINT.2022.102683.

[10] V. K. Kinra and V. R. Iyer. "Ultrasonic measurement of the thickness, phase velocity, density or attenuation of a thin-viscoelastic plate. Part I: the forward problem". *Ultrasonics* 33 (2 Jan. 1995), pp. 95–109. 0041-624X. DOI: 10.1016/0041-624X(94)00025-K.

[11] W. P. Mason and H. J. McSkimin. "Attenuation and Scattering of High Frequency Sound Waves in Metals and Glasses Energy Losses of Sound Waves in Metals Due to". *Journal of the Acoustical Society of America* 19 (1947), p. 940. DOI: 10.1121/1.1916504.

[12] W. P. Mason et al. "Measurement of Shear Elasticity and Viscosity of Liquids at Ultrasonic Frequencies". *Phys. Rev.* 75 (6 Mar. 1949), pp. 936–946. DOI: 10.1103/PhysRev.75.936.

[13] R. S. Moore and H. J. McSkimin. "Dynamic Shear Properties of Solvents and Polystyrene Solutions from 20 to 300 MHz". *Physical Acoustics* 6 (C Jan. 1970), pp. 167–242. DOI: 10.1016/B978-0-12-395666-8.50018-X.

[14] R. Saggin and J. N. Coupland. "Oil viscosity measurement by ultrasonic reflectance". *JAOCS* 78 (5 2001), pp. 509–511. DOI: 10. 1007/S11746-001-0294-Z.

[15] M. S. Greenwood and J. A. Bamberger. "Measurement of Viscosity and Shear Wave Velocity of a Liquid or Slurry for On-Line Process Control". *Ultrasonics* 39 9 (2002). DOI: 10.1016/S0041-624X(02)00372-4.

[16] V. V. Shah and K. Balasubramaniam. "Measuring Newtonian viscosity from the phase of reflected ultrasonic shear wave". *Ultrasonics* 38 (9 Sept. 2000), pp. 921–927. DOI: 10.1016/S0041-624X(00)00033-0.

[17] M. Schirru et al. "Viscosity Measurement in a Lubricant Film Using an Ultrasonically Resonating Matching Layer". *Tribology Letters* 60 (3 Dec. 2015), pp. 1–11. DOI: 10.1007/s11249-015-0619-x.

[18] G. Peretti et al. "In-situ ultrasonic viscometry of lubricants under temperature and shear". *Tribology International* (Dec. 2023), p. 109210 DOI: 10.1016/J.TRIBOINT.2023.109210.

[19] G. Peretti, N. Bouscharain, and R. Dwyer-Joyce. "In-situ ultrasonic viscometry of lubricants under high-pressure and high-shear". *Rheologica Acta* (Sept. 2025). DOI: 10.1007/s00397-025-01516-9.

[20] DuPont. Kapton® HN Polyimide Film. url: https://www.dupont.com/electronics-industrial/kapton-hn.html.

[21] Cannon Instrument. Viscosity and Flash Point Standards. Accessed: 2023–06-05. url: https://cannoninstrument.com/viscosity-flash-point-standards.html.

[22] VWR. VWR® for calibration. Accessed: 2023–06-05. 2021. url: https://uk.vwr.com/store/product/18545012/viscosity-standards.